remote sensing

MDPI

Article

A Fast PARAFAC Algorithm for Parameter Estimation in Monostatic FDA-MIMO Radar

Wenshuai Wang [1], Xiang Lan [1,*], Jinmei Shi [2] and Xianpeng Wang [1]

[1] State Key Laboratory of Marine Resource Utilization in South China Sea, School of Information and Communication Engineering, Hainan University, Haikou 570228, China; 20081000210037@hainanu.edu.cn (W.W.); wxpeng2016@hainu.edu.cn (X.W.)
[2] College of Information Engineering, Hainan Vocational University of Science and Technology, Haikou 571158, China; Shijinmei1003@hvust.edu.cn
* Correspondence: xlan@hainanu.edu.cn

Abstract: This paper studies the joint range and angle estimation of monostatic frequency diverse array multiple-input multiple-output (FDA-MIMO) radar and proposes a joint estimation algorithm. First, the transmit direction matrix is converted into real values by unitary transformation, and the Vandermonde-like matrix structure is used to construct an augmented output that doubles the aperture of the receive array. Then the augmented output is combined into a third-order tensor. Next, the factor matrices are initially estimated. Finally, the direction matrices are estimated utilizing parallel factor (PARAFAC) decomposition, and the range and angle are calculated by employing least square fitting. As contrasted with the classic PARAFAC method, the proposed method can estimate more targets and provide better estimation performance, and requires less computational complexity. The availability and excellence of the proposed method are reflected by numerical simulations and complexity analysis.

Keywords: monostatic FDA-MIMO radar; augmented output; parameter estimation; PARAFAC decomposition

check for updates

Citation: Wang, W.; Lan, X.; Shi, J.; Wang, X. A Fast PARAFAC Algorithm for Parameter Estimation in Monostatic FDA-MIMO Radar. *Remote Sens.* **2022**, *14*, 3093. https://doi.org/10.3390/rs14133093

Academic Editors: Fangqing Wen, Jin He, Veerendra Dakulagi and Wei Liu

Received: 7 May 2022
Accepted: 21 June 2022
Published: 27 June 2022

Publisher's Note: MDPI stays neutral with regard to jurisdictional claims in published maps and institutional affiliations.

Copyright: © 2022 by the authors. Licensee MDPI, Basel, Switzerland. This article is an open access article distributed under the terms and conditions of the Creative Commons Attribution (CC BY) license (https://creativecommons.org/licenses/by/4.0/).

1. Introduction

The use of parameter estimation to locate targets is a crucial part of radar target detection [1]. However, traditional radar struggles to accomplish the more accurate parameter estimation required by modern society. As a result, researchers used multiple-input multiple-output (MIMO) technology [2–5], which has had significant success in the world of communication, in the field of radar, resulting in the formation of a MIMO radar. Due to the crossed signal transmission and reception, MIMO radar generates many virtual elements in the array, which enhances degrees of freedom and parameter estimation performance significantly [6,7]. Accordingly, target localization using parameter estimation of MIMO radar has become a hot research field in academia [8]. However, since the beam pattern of MIMO radar is only influenced as a result of the angle information, two targets with unequal ranges and equal angles cannot be identified [9].

Frequency diversity array (FDA) radar was proposed by Antonik and Wicks in 2006 [10]. By adjusting the carrier frequency of each antenna [11,12], the FDA radar controls the beam forms of various range–angle relationships, providing the possibility of joint range and angle calculation for the target. For the purpose of giving MIMO radar the range-dependent beam advantages of FDA radar, researchers proposed the FDA-MIMO radar system [13,14].

Joint range–angle parameter estimation has become a popular study direction with the employment of FDA-MIMO radar. In [15], the rotational invariance technique was used to estimate parameter values for monostatic FDA-MIMO by Li B. et al. In [16], Feilong Liu proposed an improved method for estimation of signal parameters that uses rotational

invariance techniques (ESPRIT); it employs unitary transformation technology to increase the range and angle calculation accuracy of FDA-MIMO radar and decrease the complexity. However, for the joint range and angle parameter calculation, the improved ESPRIT method still suffers from the low accuracy problem. In [17], Xiong J. et al. proposed a method for parameter estimation of monostatic FDA-MIMO radar based on multiple signal classification (MUSIC). This method improves the estimation accuracy to a considerable level, but the complexity is too high to ensure efficiency in practical applications, as the algorithm involves a two-dimensional spectral peak search. The above algorithms are all algorithms based on matrix analysis, which ignores the multi-dimensional information of multi-dimensional data. To make better use of this information, researchers began to study the methods of multi-dimensional data processing.

For multi-dimensional data processing, parallel factor (PARAFAC) is a method that preserves the multidimensional structure of the data and performs well in parameter estimation [18–22]. Thus, scholars began to use the PARAFAC method to estimate the parameter values of FDA-MIMO radar [23–25]. The traditional PARAFAC algorithm randomly sets the initial values, e.g., initializing the factor matrices with Gaussian random matrices. However, setting the initial values in this way has great uncertainty and often leads to a high number of iterations for convergence, which makes the algorithm's complexity increase greatly, especially in the cases of large array numbers or high sample numbers. Consequently, how to reduce the complexity of the PARAFAC decomposition process has also become an important part of using PARAFAC. One way to decrease the complexity of PARAFAC is to employ the tensor compression technique to get a smaller tensor [26–28]. However, there exists information loss in the compression process, which causes degradation of performance. Therefore, reducing the complexity of the PARAFAC decomposition process by taking a suitable initial value also becomes a way to apply PARAFAC decomposition efficiently [29].

As the parameter estimation performance has a great relationship with the number of snapshots and the array aperture [30–34], in an attempt to increase the parameter estimation performance, many scholars began to expand the number of snapshots and the array virtual aperture of the received signal model by constructing the augmented output, so as to increase the accuracy of the parameter estimation. To better exploit the advantages of FDA-MIMO radar, the parameter calculation accuracy of the PARAFAC-like method can be improved by constructing augmented output. In this paper, we firstly propose improved fast parallel factor decomposition for joint range and angle value calculation of monostatic FDA-MIMO radar, which utilizes a structure of the signal matrix similar to that of Vandermonde to construct the augmented output, which expands the aperture of the receive array performance and improves the parameter estimation. The expansion of the receive array aperture leads to an increase in algorithm complexity. On that account, we use the idea of the propagator method (PM) [35] to obtain the initial estimated values of the factor matrices to lower the complexity of the process of the PARAFAC decomposition. Numerical simulations reflect that the proposed method is more excellent than the classic PARAFAC algorithm [23]. Utilizing the PM to reduce computational complexity does not decrease estimation performance.

For this paper, the outline is as follows. In Section 2, we introduce some tensor operations and the FDA-MIMO radar model for the parameter calculation. In Section 3, we construct the augmented output and perform the initial estimation of the factor matrices, and use parallel decomposition to estimate the angle and range. In Section 4, we report simulation experiments and performance analysis. Section 5 is the conclusion of this work.

For the notation of this paper, Table 1 gives the definitions.

Table 1. Notation of this paper.

Notations	Definitions
$(\cdot)^*$	conjugate
$(\cdot)^\dagger$	pseudo-inverse
$(\cdot)^H$	conjugate-transpose
$(\cdot)^{-1}$	inverse
$(\cdot)^T$	transpose
$\otimes$	Kronecker product
$\circ$	identity matrix the vector outer product
$\odot$	Khatri-Rao product
$\boldsymbol{D}_n(\boldsymbol{B})$	the diagonal matrix consists of the n-th row of $\boldsymbol{B}$
$\|\cdot\|_F$	the Frobenius norm
$\boldsymbol{I}_K$	$K \times K$ identity matrix
$\boldsymbol{\Pi}_n$	$M \times M$ exchange matrix
$Re(\cdot)$	the real part operator
$angle(\boldsymbol{A})$	the phase angle of $\boldsymbol{A}$

2. Tensor Operations and Signal Model

2.1. Tensor Operations

First, we describe some operations on third-order tensors related to this paper [36], taking $\boldsymbol{\mathcal{X}} \in I_1 \times I_2 \times I_3$ as an example.

Operation 1: Rank-one tensor.

$\boldsymbol{\mathcal{X}}$ is rank one if it can be formulated as:

$$\boldsymbol{\mathcal{X}} = \boldsymbol{c} \circ \boldsymbol{b} \circ \boldsymbol{a} \tag{1}$$

where $\boldsymbol{c} \in I_1 \times 1$, $\boldsymbol{b} \in I_2 \times 1$ and $\boldsymbol{a} \in I_3 \times 1$. Each element of $\boldsymbol{\mathcal{X}}$ is the multiplication of the corresponding element of the vector:

$$(\boldsymbol{c} \circ \boldsymbol{b} \circ \boldsymbol{a})_{I_1 I_2 I_3} = c_{I_1} b_{I_2} a_{I_3} \tag{2}$$

Operation 2: PARAFAC decomposition.

The PARAFAC decomposition decomposes $\boldsymbol{\mathcal{X}}$ up to the sum of the rank-one tensors.

$$\boldsymbol{\mathcal{X}} = \sum_{k=1}^{K} \boldsymbol{c}_k \circ \boldsymbol{b}_k \circ \boldsymbol{a}_k \tag{3}$$

where $\boldsymbol{c}_k$, $\boldsymbol{b}_k$ and $\boldsymbol{a}_k$ are factor matrices. The elements of $\boldsymbol{\mathcal{X}}$ are:

$$\boldsymbol{\mathcal{X}}_{I_1 I_2 I_3} = \sum_{k=1}^{K} c_{I_{1k}} b_{I_{2k}} a_{I_{3k}} \tag{4}$$

2.2. Signal Model

In this paper, all estimation work is based on monostatic FDA-MIMO radar. Assume the MIMO radar consists of M antennas in the transmitting array, and the receiving array has N antennas. Both the transmitter and receiver are designed as uniform linear arrays (ULA), and the spacing in the transmitting array d_t and the receiving array d_r is equal to one-half the wavelength. Due to the limitation of sampling technology and the physical characteristics of FDA, the receiving array cannot be frequency-controlled, so generally only the transmitting array adopts a frequency-controlled array. The construction of monostatic FDA-MIMO radar is given in Figure 1. It can be found that in the monostatic FDA-MIMO radar, the direction of arrival (DOA) is identical to the direction of departure (DOD).

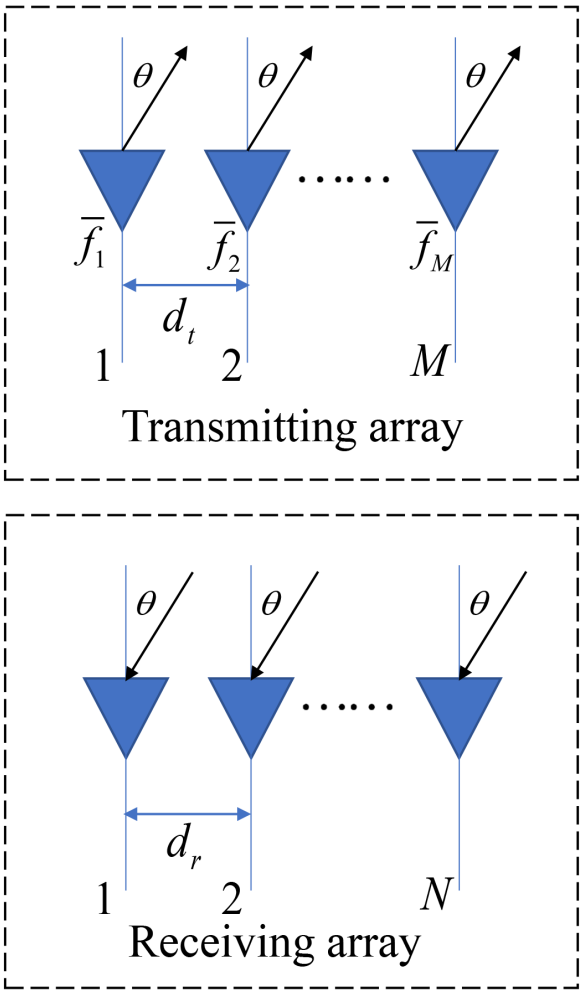


Figure 1. Monostatic FDA-MIMO radar.

Design the carrier frequency $\bar{f}_1$ of the first element as the reference frequency. Then for the m-th element, the carrier frequency is:

$$\bar{f}_m = \bar{f}_1 + (m-1)\Delta f \tag{5}$$

where Δf represents the frequency increment between adjacent array elements and $\Delta f \ll \bar{f}_1$.

The baseband signals generated by different elements of the transmitting array are orthogonal to each other; then the emission waveform of the element of the m-th element satisfies:

$$h_m(t) = Q \times \phi_m(t) e^{j2\pi \bar{f}_m t}, \quad 0 \le t \le T \tag{6}$$

where $\phi_m(t)$ denotes the baseband waveform, T represents the duration of the radar pulse, and $Q = \sqrt{E/M}$, where E denotes the overall transmitted energy.

Assume the baseband signals are all positively orthogonal to each other. Set the time delay to T, and then normalize them these signals:

$$\int_0^T \phi_m(t) \times \phi_n^*(t-\tau) e^{j2\pi\Delta f t(m-n)} dt = \begin{cases} 1, & m = n, \tau = 0 \\ 0, & m \ne n, \forall \tau \end{cases} \tag{7}$$

Suppose there are K uncorrelated narrowband stationary targets in the far-field. The range of targets far exceeds the array aperture of the monostatic FDA-MIMO radar. The range and angle of the k-th target are given by r_k and θ_k, respectively. r_k has to be confined to

the interval $(0, c/2\Delta f)$, where c represents the speed of electromagnetic wave propagation, due to the constraint of the maximum uncertainty range [37].

The transmitting array is an FDA array, so the transmitting steering vector contains angle information and range information. This steering vector is [38]:

$$\boldsymbol{a}_t(\theta_k, r_k) = \boldsymbol{b}(\theta_k) \circ \boldsymbol{r}(r_k) \tag{8}$$

where $\boldsymbol{b}(\theta_k)$ contains DOD information expressed as:

$$\boldsymbol{b}(\theta_k) = [1, e^{j2\pi \frac{d_r}{\lambda} sin\theta_k}, \cdots, e^{j2\pi(M-1)\frac{d_r}{\lambda} sin\theta_k)}]^T \tag{9}$$

$\boldsymbol{r}(r_k)$ contains range information expressed as:

$$\boldsymbol{r}(r_k) = [1, e^{-\frac{4\Delta f r_k}{c}}, \cdots, e^{-(M-1)\frac{4\Delta f r_k}{c}}]^T \tag{10}$$

Since the receiving array is not frequency control, the receiving steering vector only contains the angle information. This steering vector is [39]:

$$\boldsymbol{a}_r(\theta_k) = [1, e^{j2\pi \frac{d_r}{\lambda} sin\theta_k}, \cdots, e^{j2\pi(N-1)\frac{d_r}{\lambda} sin\theta_k)}]^T \tag{11}$$

Next, the received data of the receiver are [40]:

$$\boldsymbol{y}(t) = \sum_{k=1}^{K} \beta_k e^{j2\pi \frac{f_k t}{f_s}} \boldsymbol{a}_r(\theta_k) \boldsymbol{a}_t(\theta_k, r_k)^T \begin{bmatrix} h_1(t) \\ h_2(t) \\ \vdots \\ h_M(t) \end{bmatrix} + \bar{\boldsymbol{n}}_k \tag{12}$$

where f_s, f_k and β_k denote the pulse repeat frequency, Doppler frequency and the radar cross section (RCS), respectively.

Since the signals send by the transmitter have orthogonality, the received data are subjected to matched filtering processing, respectively. The output result of the m-th matching filter is [40]:

$$\bar{\boldsymbol{x}}_m(t) = \sum_{k=1}^{K} \beta_k e^{j2\pi \frac{f_k t}{f_s}} \boldsymbol{a}_r(\theta_k) a_{tm}(\theta_k, r_k) + \tilde{\boldsymbol{n}}_m \tag{13}$$

where $a_{tm}(\theta_k, r_k)$ is the m-th element of $\boldsymbol{a}_t(\theta_k, r_k)$.

Stack the outputs of all matched filters into a vector $\boldsymbol{x}(t) = [\bar{\boldsymbol{x}}_1^T(t), \bar{\boldsymbol{x}}_2^T(t), \cdots, \bar{\boldsymbol{x}}_M^T(t)]^T \in \mathbb{C}^{MN \times 1}$, which can be expressed as [41]:

$$\begin{aligned} \boldsymbol{x}(t) &= \sum_{k=1}^{K} (\boldsymbol{a}_r(\theta_k) \otimes \boldsymbol{a}_t(\theta_k, r_k)) + \boldsymbol{n} \\ &= (\boldsymbol{A}_R \odot \boldsymbol{A}_T)\boldsymbol{s}(t) + \boldsymbol{n} \end{aligned} \tag{14}$$

where $\boldsymbol{A}_T = [\boldsymbol{a}_t(\theta_1, r_1), \cdots, \boldsymbol{a}_t(\theta_K, r_K)]$, $\boldsymbol{A}_R = [\boldsymbol{a}_r(\theta_1), \cdots, \boldsymbol{a}_r(\theta_K)]$, and $\boldsymbol{s}(t) = [s_1(t), \cdots, s_K(t)]^T$. $s_k(t) = \beta_k e^{j2\pi f_k t/f_s}$. Assume that $\boldsymbol{a}_t(\theta_k, r_k)$, $\boldsymbol{a}_r(\theta_k)$ and the RCS are consistent for J snapshots, and $\boldsymbol{S} = [\boldsymbol{s}(1), \cdots, \boldsymbol{s}(J)]$. The received data are expressed as:

$$\boldsymbol{X} = (\boldsymbol{A}_R \odot \boldsymbol{A}_T)\boldsymbol{S} + \boldsymbol{N} \tag{15}$$

$\boldsymbol{S}$ can be expressed as:

$$\boldsymbol{S} = \begin{bmatrix} \beta_1 e^{j2\pi\frac{f_1}{f_s}} & \beta_1 e^{j4\pi\frac{f_1}{f_s}} & \cdots & \beta_1 e^{j2J\pi\frac{f_1}{f_s}} \\ \beta_2 e^{j2\pi\frac{f_2}{f_s}} & \beta_2 e^{j4\pi\frac{f_2}{f_s}} & \cdots & \beta_2 e^{j2J\pi\frac{f_2}{f_s}} \\ \vdots & \vdots & \ddots & \vdots \\ \beta_K e^{j2\pi\frac{f_K}{f_s}} & \beta_K e^{j4\pi\frac{f_K}{f_s}} & \cdots & \beta_K e^{j2J\pi\frac{f_K}{f_s}} \end{bmatrix} \tag{16}$$

Each row of the signal matrix $\boldsymbol{S}$ has a structure similar to the Vandermonde matrix, as can be seen.

3. Improved Fast Parallel Factorization Algorithm

3.1. Construction of Augmented Output

The section obtains an augmented output whose receiving array aperture is twice that of the original signal, which improves the maximum number of identifiable targets [34] and the parameter estimation performance.

Let $\boldsymbol{U}_M$ be the unitary matrix. When M is odd, the unitary matrix is [42]:

$$\boldsymbol{U}_M = \frac{1}{\sqrt{2}} \begin{bmatrix} \boldsymbol{I}_k & 0 & j\boldsymbol{I}_k \\ 0 & \sqrt{2} & 0 \\ \boldsymbol{\Pi}_k & 0 & -j\boldsymbol{\Pi}_k \end{bmatrix} \tag{17}$$

where $M = 2k + 1$.

When M is even, the unitary matrix is:

$$\boldsymbol{U}_M = \frac{1}{\sqrt{2}} \begin{bmatrix} \boldsymbol{I}_k & j\boldsymbol{I}_k \\ \boldsymbol{\Pi}_k & -j\boldsymbol{\Pi}_k \end{bmatrix} \tag{18}$$

where $M = 2k$.

The transmitting steering vector can instead be rewritten as:

$$\boldsymbol{a}_t(\theta_k, r_k) = [1, e^{j2\pi(\frac{d_t}{\lambda}sin\theta_k - \frac{2\Delta f r_k}{c})}, \cdots, e^{j2\pi(M-1)(\frac{d_t}{\lambda}sin\theta_k - \frac{2\Delta f r_k}{c})}]^T \tag{19}$$

Assuming that M is odd, $\boldsymbol{U}_M\boldsymbol{a}_t(\theta_k, r_k)$ is:

$$\boldsymbol{U}_M\boldsymbol{a}_t(\theta_k, r_k) = \sqrt{2}e^{j\pi(M-1)(\frac{d_t}{\lambda}sin\theta_k - \frac{2\Delta f r_k}{c})} \times \begin{bmatrix} cos(\pi(M-1)(\frac{d_t}{\lambda}sin\theta_k - \frac{2\Delta f r_k}{c})) \\ \vdots \\ cos(\pi(\frac{d_t}{\lambda}sin\theta_k - \frac{2\Delta f r_k}{c})) \\ \frac{1}{\sqrt{2}} \\ -sin(\pi(M-1)(\frac{d_t}{\lambda}sin\theta_k - \frac{2\Delta f r_k}{c})) \\ \vdots \\ -sin(\pi(\frac{d_t}{\lambda}sin\theta_k - \frac{2\Delta f r_k}{c})) \end{bmatrix} \tag{20}$$

Define

$$\boldsymbol{a}_t^r(\theta_k, r_k) = \sqrt{2} \times \begin{bmatrix} cos(\pi(M-1)(\frac{d_t}{\lambda}sin\theta_k - \frac{2\Delta f r_k}{c})) \\ \vdots \\ cos(\pi(\frac{d_t}{\lambda}sin\theta_k - \frac{2\Delta f r_k}{c})) \\ \frac{1}{\sqrt{2}} \\ -sin(\pi(M-1)(\frac{d_t}{\lambda}sin\theta_k - \frac{2\Delta f r_k}{c})) \\ \vdots \\ -sin(\pi(\frac{d_t}{\lambda}sin\theta_k - \frac{2\Delta f r_k}{c})) \end{bmatrix} \tag{21}$$

Define $\boldsymbol{U} = \boldsymbol{I}_N \bigotimes \boldsymbol{U}_M$ and $u_k = e^{j\pi(M-1)(\frac{d_t}{\lambda}sin\theta_k - \frac{2\Delta fr_k}{c})}$. According to Equations (20) and (21), the direction steering vector is transformed by:

$$\begin{aligned}
&\boldsymbol{U}^H(\boldsymbol{a}_r(\theta_k) \otimes \boldsymbol{a}_t(\theta_k, r_k)) \\
&= (\boldsymbol{I}_N \otimes \boldsymbol{U}_M^H)(\boldsymbol{a}_r(\theta_k) \otimes \boldsymbol{a}_t(\theta_k, r_k)) \\
&= (\boldsymbol{I}_N \times \boldsymbol{a}_r(\theta_k)) \otimes (\boldsymbol{U}_M \boldsymbol{a}_t(\theta_k, r_k)) \\
&= \boldsymbol{a}_r(\theta_k) \otimes (e^{j\pi(M-1)(\frac{d_t}{\lambda}sin\theta_k - \frac{2\Delta fr_k}{c})} \times \boldsymbol{a}_t^r(\theta_k, r_k)) \\
&= \boldsymbol{a}_r(\theta_k) \otimes (u_k \boldsymbol{a}_t^r(\theta_k, r_k)) \\
&= u_k \boldsymbol{a}_r(\theta_k) \otimes \boldsymbol{a}_t^r(\theta_k, r_k)
\end{aligned} \tag{22}$$

Define the direction matrix as $\boldsymbol{A} = [\boldsymbol{a}_r(\theta_1) \otimes \boldsymbol{a}_t(\theta_1, r_1), \cdots, \boldsymbol{a}_r(\theta_K) \otimes \boldsymbol{a}_t(\theta_K, r_K)]$. According to Equation (22), the direction matrix can be transformed by:

$$\boldsymbol{A}_U = \boldsymbol{U}^H \boldsymbol{A} = [u_1 \boldsymbol{a}_r(\theta_1) \otimes \boldsymbol{a}_t^r(\theta_1, r_1), \cdots, u_K \boldsymbol{a}_r(\theta_K) \otimes \boldsymbol{a}_t^r(\theta_K, r_K)] \tag{23}$$

The received data can be transformed by:

$$\boldsymbol{X}_U = \boldsymbol{U}^H \boldsymbol{X} = \boldsymbol{U}^H \boldsymbol{A} \boldsymbol{S} = \boldsymbol{A}_U \boldsymbol{S} \tag{24}$$

According to Equation (16), the following formula is obtained:

$$\boldsymbol{S}^* \boldsymbol{\Pi}_J = \boldsymbol{\psi} \boldsymbol{S} \tag{25}$$

where $\boldsymbol{\psi} = diag(\alpha_1, \ldots, \alpha_K)$ where $\alpha_k = \frac{\beta_k^*}{\beta_k} e^{-j2\pi \frac{f_k(J+1)}{f_s}}, k = 1, \cdots, K$.

Let $\boldsymbol{X}_C = \boldsymbol{X}_U^* \boldsymbol{\Pi}_J = \boldsymbol{A}_U^* \boldsymbol{\psi} \boldsymbol{S}$. The augmented output can be constructed as [34]:

$$\begin{aligned}
\boldsymbol{X}_E &= \begin{bmatrix} \boldsymbol{X}_U \\ \boldsymbol{X}_C \end{bmatrix} = \begin{bmatrix} \boldsymbol{A}_U \\ \boldsymbol{A}_U^* \boldsymbol{\psi} \end{bmatrix} \boldsymbol{S} \\
&= \begin{bmatrix} u_1 \boldsymbol{a}_r(\theta_1) \otimes \boldsymbol{a}_t^r(\theta_1, r_1) & \cdots & u_K \boldsymbol{a}_r(\theta_K) \otimes \boldsymbol{a}_t^r(\theta_K, r_K) \\ \alpha_1 u_1^* \boldsymbol{a}_r^*(\theta_1) \otimes \boldsymbol{a}_t^r(\theta_1, r_1) & \cdots & \alpha_K u_K^* \boldsymbol{a}_r^*(\theta_K) \otimes \boldsymbol{a}_t^r(\theta_K, r_K) \end{bmatrix} \boldsymbol{S} \\
&= \begin{bmatrix} \boldsymbol{a}_e(\theta_1) \otimes \boldsymbol{a}_t^r(\theta_1, r_1) & \cdots & \boldsymbol{a}_e(\theta_K) \otimes \boldsymbol{a}_t^r(\theta_K, r_K) \end{bmatrix}
\end{aligned} \tag{26}$$

where $\boldsymbol{a}_e(\theta_k) = [u_k \boldsymbol{a}_r^T(\theta_k), \alpha_k u_k^* \boldsymbol{a}_r^H(\theta_k)]^T$.

According to Equation (26), the receive direction matrix of the augmented output is:

$$\begin{aligned}
\boldsymbol{A}_E &= \begin{bmatrix} \boldsymbol{a}_e(\theta_1) & \cdots & \boldsymbol{a}_e(\theta_K) \end{bmatrix} \\
&= \begin{bmatrix} u_1 \boldsymbol{a}_r(\theta_1) & \cdots & u_K \boldsymbol{a}_r(\theta_K) \\ \alpha_1 u_1^* \boldsymbol{a}_r^*(\theta_1) & \cdots & \alpha_K u_K^* \boldsymbol{a}_r^*(\theta_K) \end{bmatrix} \in \mathbb{C}^{2N \times K}
\end{aligned} \tag{27}$$

The transmit direction matrix of the augmented output is:

$$\boldsymbol{A}_F = [\boldsymbol{a}_t^r(\theta_1, r_1), \cdots, \boldsymbol{a}_t^r(\theta_K, r_K)] \in \mathbb{C}^{M \times K} \tag{28}$$

According to Equations (27) and (28), Equation (26) can be modified as:

$$\begin{aligned}
\boldsymbol{X}_E &= \begin{bmatrix} \boldsymbol{X}_1 \\ \boldsymbol{X}_2 \\ \vdots \\ \boldsymbol{X}_{2N} \end{bmatrix} = \begin{bmatrix} \boldsymbol{A}_F D_1(\boldsymbol{A}_E) \\ \boldsymbol{A}_F D_2(\boldsymbol{A}_E) \\ \vdots \\ \boldsymbol{A}_F D_{2N}(\boldsymbol{A}_E) \end{bmatrix} \boldsymbol{S} + \begin{bmatrix} \boldsymbol{N}_{x1} \\ \boldsymbol{N}_{x2} \\ \vdots \\ \boldsymbol{N}_{x2N} \end{bmatrix} \\
&= (\boldsymbol{A}_E \odot \boldsymbol{A}_F) \boldsymbol{S} + \boldsymbol{N}_x
\end{aligned} \tag{29}$$

where $\boldsymbol{X}_n$ is

$$\boldsymbol{X}_n = \boldsymbol{A}_F D_n(\boldsymbol{A}_E) \tag{30}$$

Under the influence of noise, the model of the augmented output is:

$$\tilde{\boldsymbol{X}}_{En} = \boldsymbol{A}_F D_n(\boldsymbol{A}_E) + \boldsymbol{N}_{xn}, \quad n = 1, 2, \cdots, 2N \tag{31}$$

According to the trilinear model [39], the tensor of the augmented output is:

$$\begin{aligned} \boldsymbol{\mathcal{X}}_{n,m,j} &= \sum_{k=1}^{K} \boldsymbol{A}_F(m,k) \circ \boldsymbol{A}_E(n,k) \circ \boldsymbol{S}(j,k) + \boldsymbol{N}_{n,m,j} \\ m &= 1, \cdots, M, n = 1, \cdots, 2N, j = 1, \cdots, J \end{aligned} \tag{32}$$

Depending on the matrix expansion of the tensor, the matrix $\boldsymbol{Y}$ is [43]:

$$\begin{aligned} \boldsymbol{Y} &= \begin{bmatrix} \boldsymbol{Y}_1 \\ \boldsymbol{Y}_2 \\ \vdots \\ \boldsymbol{Y}_M \end{bmatrix} = \begin{bmatrix} \boldsymbol{S}^T D_1(\boldsymbol{A}_F) \\ \boldsymbol{S}^T D_2(\boldsymbol{A}_F) \\ \vdots \\ \boldsymbol{S}^T D_M(\boldsymbol{A}_F) \end{bmatrix} \boldsymbol{A}^E + \begin{bmatrix} \boldsymbol{N}_{y1} \\ \boldsymbol{N}_{y2} \\ \vdots \\ \boldsymbol{N}_{yM} \end{bmatrix} \\ &= (\boldsymbol{A}_F \odot \boldsymbol{S}^T)\boldsymbol{A}_E^T + \boldsymbol{N}_y \end{aligned} \tag{33}$$

The matrix $\boldsymbol{Z}$ is [43]:

$$\begin{aligned} \boldsymbol{Z} &= \begin{bmatrix} \boldsymbol{Z}_1 \\ \boldsymbol{Z}_2 \\ \vdots \\ \boldsymbol{Z}_J \end{bmatrix} = \begin{bmatrix} \boldsymbol{A}^E D_1(\boldsymbol{S}^T) \\ \boldsymbol{A}^E D_2(\boldsymbol{S}^T) \\ \vdots \\ \boldsymbol{A}^E D_J(\boldsymbol{S}^T) \end{bmatrix} \boldsymbol{A}^F + \begin{bmatrix} \boldsymbol{N}_{z1} \\ \boldsymbol{N}_{z2} \\ \vdots \\ \boldsymbol{N}_{zJ} \end{bmatrix} \\ &= (\boldsymbol{S}^T \odot \boldsymbol{A}_E)\boldsymbol{A}_F^T + \boldsymbol{N}_z \end{aligned} \tag{34}$$

3.2. Initial Estimation of Factor Matrix

The PARAFAC technique usually employs the trilinear alternating least squares (TALS) method to directly decompose the obtained model. However, the traditional TALS algorithm directly uses random initial values to iterate, which often leads to slow convergence of the iterative decomposition process, which increases the complexity of the algorithm. The receiving array aperture was expanded by a factor of two in the previous section, considerably increasing the complexity of each iteration in the trilinear decomposition process. To decrease the complexity of trilinear decomposition, we used the PM idea for initial estimation of factor matrices, with scale variation to get better initial values, reduce the number of parallel factor iterations and decrease the complexity in the trilinear decomposition process.

After elementary row transformation, the reconstructed received augmented output $\boldsymbol{X}_E'$ can be expressed as:

$$\boldsymbol{X}_E' = \boldsymbol{G}\boldsymbol{X}_E = (\boldsymbol{A}_F \odot \boldsymbol{A}_E)\boldsymbol{S} + \boldsymbol{N}' = \begin{bmatrix} \boldsymbol{A}_E D_1(\boldsymbol{A}_F) \\ \boldsymbol{A}_E D_2(\boldsymbol{A}_F) \\ \vdots \\ \boldsymbol{A}_E D_M(\boldsymbol{A}_F) \end{bmatrix} + \boldsymbol{N}' \tag{35}$$

where $\boldsymbol{G} \in \mathbb{C}^{2NM \times 2NM}$ is the row transformation matrix, which can be expressed as:

$$\boldsymbol{G} = \begin{bmatrix} \left\{ \begin{matrix} \overbrace{10\cdots0}^{M} & & & \\ & \overbrace{10\cdots0}^{M} & & \\ & & \ddots & \\ & & & \overbrace{10\cdots0}^{M} \end{matrix} \right\} 2N \\ \left\{ \begin{matrix} \overbrace{01\cdots0}^{M} & & & \\ & \overbrace{01\cdots0}^{M} & & \\ & & \ddots & \\ & & & \overbrace{01\cdots0}^{M} \end{matrix} \right\} 2N \\ \vdots \\ \left\{ \begin{matrix} \overbrace{00\cdots1}^{M} & & & \\ & \overbrace{00\cdots1}^{M} & & \\ & & \ddots & \\ & & & \overbrace{00\cdots1}^{M} \end{matrix} \right\} 2N \end{bmatrix} \tag{36}$$

Define $\boldsymbol{V} = \boldsymbol{A}_F \odot \boldsymbol{A}_E$. It is divided into two parts:

$$\boldsymbol{V} = \begin{bmatrix} \boldsymbol{V}_{1K} \\ \boldsymbol{V}_{2K} \end{bmatrix} = \begin{bmatrix} \boldsymbol{I}_K \\ \boldsymbol{P}^T \end{bmatrix} \boldsymbol{V}_{1K} \tag{37}$$

where $\boldsymbol{V}_{1K} \in \mathbb{C}^{K\times K}$, $\boldsymbol{V}_{2K} \in \mathbb{C}^{(2MN-K)\times K}$, $\boldsymbol{P} \in \mathbb{C}^{(2MN-K)\times K}$ and $\boldsymbol{I}_K$ is the $K \times K$ identity matrix.

Let $\boldsymbol{P}_c$ be:

$$\boldsymbol{P}_c = \begin{bmatrix} \boldsymbol{I}_K \\ \boldsymbol{P}^T \end{bmatrix} \tag{38}$$

Then the following relationship can be obtained:

$$\boldsymbol{P}_c \boldsymbol{V}_{1K} = \boldsymbol{V} \tag{39}$$

For the reconstructed received augmented output $\boldsymbol{X}'_E$, the covariance matrix is:

$$\begin{aligned} \boldsymbol{R} &= E[\boldsymbol{X}'_E \boldsymbol{X}'^H_E] = (\boldsymbol{A}_F \odot \boldsymbol{A}_E) E[\boldsymbol{S}\boldsymbol{S}^H] (\boldsymbol{A}_F \odot \boldsymbol{A}_E)^H + E[\boldsymbol{N}'\boldsymbol{N}'^H] \\ &= (\boldsymbol{A}_F \odot \boldsymbol{A}_E) \boldsymbol{R}_S (\boldsymbol{A}_F \odot \boldsymbol{A}_E)^H + \boldsymbol{R}_N \\ &= (\boldsymbol{A}_F \odot \boldsymbol{A}_E) \boldsymbol{R}_C + \boldsymbol{R}_N = \boldsymbol{V}\boldsymbol{R}_C + \boldsymbol{R}_N \end{aligned} \tag{40}$$

where $\boldsymbol{R}_C = \boldsymbol{R}_S (\boldsymbol{A}_F \odot \boldsymbol{A}_E)^H$.

The matrix $\boldsymbol{R}$ is partitioned by:

$$\begin{aligned} \boldsymbol{R} &= \begin{bmatrix} \boldsymbol{R}_1 \\ \boldsymbol{R}_2 \end{bmatrix} = \begin{bmatrix} \boldsymbol{V}_{1K} \\ \boldsymbol{V}_{2K} \end{bmatrix} \boldsymbol{R}_C + \boldsymbol{R}_N \\ &= \begin{bmatrix} \boldsymbol{I}_K \\ \boldsymbol{P}^T \end{bmatrix} \boldsymbol{V}_{1K} + \boldsymbol{R}_N \end{aligned} \tag{41}$$

where $\boldsymbol{R}_1 \in \mathbb{C}^{2MN\times K}$; $\boldsymbol{R}_2 \in \mathbb{C}^{2MN\times(2MN-K)}$. Without noise, $\boldsymbol{R}_1$ and $\boldsymbol{R}_2$ satisfy:

$$\boldsymbol{R}_2 = \boldsymbol{P}^T\boldsymbol{R}_1 \tag{42}$$

In application, the covariance matrix $\boldsymbol{R}$ is:

$$\hat{\boldsymbol{R}} = \boldsymbol{X}'_E\boldsymbol{X}'^H_E/J \tag{43}$$

The estimate of the matrix $\boldsymbol{P}$ is the minimum of the following equation:

$$\bar{J}_{csm}(\boldsymbol{P}) = \|\hat{\boldsymbol{R}}_2 - \boldsymbol{P}^T\hat{\boldsymbol{R}}_1\|_F^2 \tag{44}$$

The estimate of $\boldsymbol{P}$ is:

$$\hat{\boldsymbol{P}} = (\hat{\boldsymbol{R}}_1^H\hat{\boldsymbol{R}}_1)^{-1}\hat{\boldsymbol{R}}_1^H\hat{\boldsymbol{R}}_2 \tag{45}$$

According to Equation (38), the estimate of $\hat{\boldsymbol{P}}_c$ can be obtained:

$$\hat{\boldsymbol{P}}_c = \begin{bmatrix} \boldsymbol{I}_K \\ \hat{\boldsymbol{P}}^T \end{bmatrix} \tag{46}$$

Then, the matrix $\hat{\boldsymbol{P}}_c$ is partitioned by:

$$\hat{\boldsymbol{P}}_c = \begin{bmatrix} \hat{\boldsymbol{P}}_1 \\ \hat{\boldsymbol{P}}_2 \\ \vdots \\ \hat{\boldsymbol{P}}_M \end{bmatrix} \tag{47}$$

According to $\boldsymbol{P}_c\boldsymbol{V}_{1K} = \boldsymbol{V}$ and $\boldsymbol{V} = \boldsymbol{A}_F \odot \boldsymbol{A}_E$, the following formulas are obtained:

$$\boldsymbol{P}_1\boldsymbol{V}_{1K} = \boldsymbol{A}_E D_1(\boldsymbol{A}_F) \tag{48}$$

$$\boldsymbol{P}_2\boldsymbol{V}_{1K} = \boldsymbol{A}_E D_2(\boldsymbol{A}_F) \tag{49}$$

There are scale ambiguity and permutation ambiguity in the PARAFAC decomposition, namely, $\tilde{\boldsymbol{A}}_F = \boldsymbol{A}_F\boldsymbol{\Gamma}\boldsymbol{\Lambda}_1$, $\tilde{\boldsymbol{A}}_E = \boldsymbol{A}_E\boldsymbol{\Gamma}\boldsymbol{\Lambda}_2$, $\tilde{\boldsymbol{S}} = \boldsymbol{S}\boldsymbol{\Gamma}\boldsymbol{\Lambda}_3$, where $\boldsymbol{\Lambda}_1\boldsymbol{\Lambda}_2\boldsymbol{\Lambda}_3 = \boldsymbol{I}$. Assume $\boldsymbol{\Lambda}_2 = D_1(\boldsymbol{A}_F)$, $\boldsymbol{\Lambda}_1 = 1/D_1(\boldsymbol{A}_F)$, $\boldsymbol{\Lambda}_3 = \boldsymbol{I}$, $\tilde{\boldsymbol{A}}_E$ and $\tilde{\boldsymbol{A}}_F$ can be expressed as:

$$\tilde{\boldsymbol{A}}_E = \boldsymbol{A}_E D_1(\boldsymbol{A}_F) \tag{50}$$

$$\tilde{\boldsymbol{A}}_F = \frac{\boldsymbol{A}_F}{D_1(\boldsymbol{A}_F)} \tag{51}$$

Equation (48) can be reformulated as:

$$\boldsymbol{P}_1\boldsymbol{V}_{1K} = \tilde{\boldsymbol{A}}_E \tag{52}$$

Equation (49) can be reformulated as:

$$\boldsymbol{P}_2\boldsymbol{V}_{1K} = \tilde{\boldsymbol{A}}_E D_2(\tilde{\boldsymbol{A}}_F) \tag{53}$$

According to Equations (52) and (53), the following formula is obtained:

$$\boldsymbol{P}_2\boldsymbol{V}_{1K} = \boldsymbol{P}_1\boldsymbol{V}_{1K}D_2(\tilde{\boldsymbol{A}}_F) \tag{54}$$

By transforming Equation (54), we get:

$$\boldsymbol{P}_1^\dagger\boldsymbol{P}_2 = \boldsymbol{V}_{1K}D_2(\tilde{\boldsymbol{A}}_F)\boldsymbol{V}_{1K}^{-1} \tag{55}$$

The eigenvalue decomposition of $\boldsymbol{P}_1^{\dagger}\boldsymbol{P}_2$ is performed to obtain the estimated $D_2(\hat{\tilde{\boldsymbol{A}}}_F)$ of $D_2(\tilde{\boldsymbol{A}}_F)$ and the estimated $\hat{\boldsymbol{V}}_{1K}$ of $\boldsymbol{V}_{1K}$. By Equation (39), the estimated $\hat{\boldsymbol{V}} = \hat{\boldsymbol{P}}_c\hat{\boldsymbol{V}}_{1K}$ of $\boldsymbol{V}$ can be obtained. Next, $\hat{\boldsymbol{V}}$ is partitioned by:

$$\hat{\boldsymbol{V}} = \begin{bmatrix} \boldsymbol{V}_1 \\ \boldsymbol{V}_2 \\ \vdots \\ \boldsymbol{V}_M \end{bmatrix} = \begin{bmatrix} \hat{\tilde{\boldsymbol{A}}}_E \\ \hat{\tilde{\boldsymbol{A}}}_E D_2(\hat{\tilde{\boldsymbol{A}}}_F) \\ \vdots \\ \hat{\tilde{\boldsymbol{A}}}_E D_M(\hat{\tilde{\boldsymbol{A}}}_F) \end{bmatrix} \tag{56}$$

where the matrices $\boldsymbol{V}_1, \boldsymbol{V}_2, \cdots, \boldsymbol{V}_M$ are all of the size $2N \times K$. From Equation (56), we can get the initial estimate $\hat{\tilde{\boldsymbol{A}}}_{Eini} = \boldsymbol{V}_1$ of $\tilde{\boldsymbol{A}}_E$, and we can also get $\boldsymbol{V}_3 = \boldsymbol{V}_1 D_3(\tilde{\boldsymbol{A}}_F)$, $\boldsymbol{V}_4 = \boldsymbol{V}_1 D_4(\tilde{\boldsymbol{A}}_F), \cdots, \boldsymbol{V}_4 = \boldsymbol{V}_1 D_M(\tilde{\boldsymbol{A}}_F)$. Subsequently, estimates of $D_3(\tilde{\boldsymbol{A}}_F), D_4(\tilde{\boldsymbol{A}}_F), \cdots, D_M(\tilde{\boldsymbol{A}}_F)$ can be obtained:

$$\begin{aligned} D_3(\tilde{\boldsymbol{A}}_F) &= \boldsymbol{V}_1^{\dagger}\boldsymbol{V}_3 \\ D_4(\tilde{\boldsymbol{A}}_F) &= \boldsymbol{V}_1^{\dagger}\boldsymbol{V}_4 \\ &\vdots \\ D_M(\tilde{\boldsymbol{A}}_F) &= \boldsymbol{V}_1^{\dagger}\boldsymbol{V}_M \end{aligned} \tag{57}$$

Owing to $\tilde{\boldsymbol{A}}_F = \boldsymbol{A}_F D_1(\boldsymbol{A}_F)$, the first row of $\tilde{\boldsymbol{A}}_F$ are all 1. We can obtain the initial estimate $\hat{\tilde{\boldsymbol{A}}}_{Fini}$ of $\tilde{\boldsymbol{A}}_F$.

According to $\boldsymbol{X}'_E = \boldsymbol{G}\boldsymbol{X}_E = (\boldsymbol{A}_F \odot \boldsymbol{A}_E)\boldsymbol{S}$, the initial estimate of $\boldsymbol{S}$ is

$$\hat{\boldsymbol{S}}_{ini} = (\hat{\tilde{\boldsymbol{A}}}_{Fini} \odot \hat{\tilde{\boldsymbol{A}}}_{Eini})^{\dagger}\boldsymbol{X}'_E \tag{58}$$

3.3. Trilinear Decomposition

The receive and transmit direction matrices are estimated by employing the TALS method in this Section [18].

Depending on Equation (29), the least square (LS) fitting is:

$$\min_{\boldsymbol{A}_E, \boldsymbol{A}_F, \boldsymbol{S}} \|\tilde{\boldsymbol{X}}_E - (\boldsymbol{A}_E \odot \boldsymbol{A}_F)\boldsymbol{S}\|_F \tag{59}$$

The LS of matrix $\boldsymbol{S}$ is estimated as:

$$\hat{\boldsymbol{S}} = (\hat{\boldsymbol{A}}_E \odot \hat{\boldsymbol{A}}_F)^{\dagger}\boldsymbol{X}_E \tag{60}$$

where $\hat{\boldsymbol{A}}_E$ represents the former estimates of $\boldsymbol{A}_E$ and $\hat{\boldsymbol{A}}_F$ represents the former estimates of $\boldsymbol{A}_F$.

Depending on Equation (33), the LS fitting is:

$$\min_{\boldsymbol{A}_E, \boldsymbol{A}_F, \boldsymbol{S}} \|\hat{\boldsymbol{Y}} - (\boldsymbol{A}_F \odot \boldsymbol{S}^T)\boldsymbol{A}_E^T\|_F \tag{61}$$

The LS of matrix $\boldsymbol{A}_E$ is estimated as:

$$\hat{\boldsymbol{A}}_E^T = (\hat{\boldsymbol{A}}_F^T \odot \hat{\boldsymbol{S}}^T)^{\dagger}\hat{\boldsymbol{Y}} \tag{62}$$

where $\hat{\boldsymbol{A}}_F$ represents the former estimates of $\boldsymbol{A}_F$ and $\hat{\boldsymbol{S}}$ represents the former estimates of $\boldsymbol{S}$.

Depending on Equation (34), the LS fitting is:

$$\min_{\boldsymbol{A}_E, \boldsymbol{A}_F, \boldsymbol{S}} \|\hat{\boldsymbol{Z}} - (\boldsymbol{S}^T \odot \boldsymbol{A}_E)\boldsymbol{A}_F^T\|_F \tag{63}$$

The LS of matrix $\boldsymbol{A}_E$ is estimated as:

$$\hat{\boldsymbol{A}}_F^T = (\hat{\boldsymbol{S}}^T \odot \hat{\boldsymbol{A}}_E^T)^\dagger \hat{\boldsymbol{Z}} \tag{64}$$

where $\hat{\boldsymbol{A}}_E$ represents the former estimates of $\boldsymbol{A}_E$ and $\hat{\boldsymbol{S}}$ represents the former estimates of $\boldsymbol{S}$.

In this section, we set the initial values as $\hat{\boldsymbol{A}}_F = \hat{\tilde{\boldsymbol{A}}}_{Fini}$, $\hat{\boldsymbol{A}}_E = \hat{\tilde{\boldsymbol{A}}}_{Eini}$, and $\hat{\boldsymbol{S}} = \hat{\boldsymbol{S}}_{ini}$. Then, iteratively update according to Equations (60), (62) and (64) until convergence.

3.4. Angle and Range Estimation

By TALS method, the final transmit direction matrix $\hat{\boldsymbol{A}}_F$ and receive direction matrix $\hat{\boldsymbol{A}}_E$ with scale ambiguity and permutation ambiguity can be obtained. Permutation ambiguity does not affect angle and range estimation; normalization can be used to resolve scale ambiguity.

After resolving the scale ambiguity, the range and angle estimated values can be obtained by the LS fitting. $\boldsymbol{a}_{Ek}$ and $\boldsymbol{a}_{Fk}$ stand for k-th column of $\boldsymbol{A}_E$ and $\boldsymbol{A}_F$, respectively. We can get:

$$\begin{aligned} \boldsymbol{h}_{Ek} = angle(normal(\boldsymbol{a}_{Ek})) = [0, 2\pi\frac{d_r}{\lambda}sin\theta_k, \cdots, 2\pi\frac{d_r}{\lambda}(N-1)sin\theta_k, \\ k, k - 2\pi\frac{d_r}{\lambda}sin\theta_k, \cdots, k - 2\pi\frac{d_r}{\lambda}(N-1)sin\theta_k]^T \end{aligned} \tag{65}$$

$$\begin{aligned} \boldsymbol{h}_{Fk} = angle(normal(\boldsymbol{U}_M\boldsymbol{a}_{Fk})) = [0, 2\pi(\frac{d_t}{\lambda}sin\theta_k - \frac{2\Delta fr_k}{c}), \\ \cdots, 2\pi(M-1)(\frac{d_t}{\lambda}sin\theta_k - \frac{2\Delta fr_k}{c})]^T \end{aligned} \tag{66}$$

where $k = angle(\alpha_k(u_k^*)^2)$, and *normal* stands for normalization.

Divide $\boldsymbol{A}_E$ into two parts to fit:

$$\boldsymbol{P}_{E1}\boldsymbol{v}_{Ek1} = \hat{\boldsymbol{h}}_{Ek1} \tag{67}$$

$$\boldsymbol{P}_{E1}\boldsymbol{v}_{Ek2} = \hat{\boldsymbol{h}}_{Ek2} \tag{68}$$

where $\hat{\boldsymbol{h}}_{Ek1}$ and $\hat{\boldsymbol{h}}_{Ek2}$ represent the first and last N rows of $\boldsymbol{h}_{Ek}$.

Define

$$\boldsymbol{P}_{E1} = \begin{bmatrix} 0 & 0 & \cdots & 0 \\ 0 & 2\pi\frac{d_r}{\lambda} & \cdots & 2\pi\frac{d_r}{\lambda}(N-1) \end{bmatrix} \in \mathbb{C}^{N\times 2} \tag{69}$$

$$\boldsymbol{P}_{E2} = \begin{bmatrix} 0 & 0 & \cdots & 0 \\ 0 & -2\pi\frac{d_r}{\lambda} & \cdots & -2\pi\frac{d_r}{\lambda}(N-1) \end{bmatrix} \in \mathbb{C}^{N\times 2} \tag{70}$$

For $\boldsymbol{v}_{Ek1}$, the LS solution is as follows:

$$\hat{\boldsymbol{v}}_{Ek1} = ({\boldsymbol{P}_{E1}}^T\boldsymbol{P}_{E1})^{-1}\boldsymbol{P}_{E1}^T\hat{\boldsymbol{h}}_{Ek1} \tag{71}$$

For $\boldsymbol{v}_{Ek2}$, the LS solution is as follows:

$$\hat{\boldsymbol{v}}_{Ek2} = (\boldsymbol{P}_{E2}^T\boldsymbol{P}_{E2})^{-1}\boldsymbol{P}_{E2}^T\hat{\boldsymbol{h}}_{Ek2} \tag{72}$$

The estimated value of the angle θ_k is:

$$\theta_k = \frac{(arcsin(\hat{\boldsymbol{v}}_{Ek1}) + arcsin(\hat{\boldsymbol{v}}_{Ek2}))}{2} \tag{73}$$

The LS fit to $\boldsymbol{A}_F$ is given by:

$$\boldsymbol{P}_t\boldsymbol{v}_{tk} = \hat{\boldsymbol{h}}_{tk} \tag{74}$$

Define

$$\boldsymbol{P}_t = \begin{bmatrix} 0 & 0 & \cdots & 0 \\ 0 & 2\pi\frac{d_t}{\lambda} & \cdots & 2\pi\frac{d_t}{\lambda}(M-1) \end{bmatrix} \in \mathbb{C}^{M\times 2} \tag{75}$$

For $\hat{\boldsymbol{v}}_{tk}$, the LS solution is as follows:

$$\hat{\boldsymbol{v}}_{tk} = \left(\boldsymbol{P}_t^T \boldsymbol{P}_t\right)^{-1} \boldsymbol{P}_t^T \hat{\boldsymbol{h}}_{tk} \tag{76}$$

The estimated value of the range r_k is:

$$r_k = \frac{\frac{d_t}{\lambda} sin(\theta_k) - \hat{\boldsymbol{v}}_{tk}(2)}{2\Delta f} \times c \tag{77}$$

The following are the major steps in the proposed method:

Step 1: According to Equations (24) and (26), obtain the augmented matrix $\boldsymbol{X}_E$;
Step 2: According to Equation (35), obtain the reconstructed received augmented output $\boldsymbol{X}_E'$;
Step 3: Get the covariance matrix $\hat{\boldsymbol{R}}$ via Equation (43);
Step 4: The propagation operator $\hat{\boldsymbol{P}}$ is obtained by Equation (45);
Step 5: Estimate initial estimate $\hat{\hat{\boldsymbol{A}}}_{Eini}$ with scale variation via Equations (55) and (56);
Step 6: Estimate initial estimate $\hat{\hat{\boldsymbol{A}}}_{Fini}$ with scale variation via Equations (56) and (57);
Step 7: Estimate initial estimate $\hat{\boldsymbol{S}}_{ini}$ with scale variation via Equation (58);
Step 8: According to Equation (32), obtain the third-order tensor $\boldsymbol{\mathcal{X}}$;
Step 9: According to Equations (60), (62) and (64), obtain the direction matrices estimates $\hat{\boldsymbol{A}}_E$ and $\hat{\boldsymbol{A}}_F$ by iterative update;
Step 10: Calculate angle via Equation (73);
Step 11: Calculate range via Equation (77);

3.5. CRB

Depending on [17], the Cramér–Rao Bound(CRB) for monostatic FDA-MIMO angle and range estimation can be calculated by:

$$\mathbf{CRB} = \frac{\sigma^2}{2J}\{Re[(\boldsymbol{W}^H \boldsymbol{P}_{\frac{1}{\hat{A}}} \boldsymbol{W}) \circ \boldsymbol{F}^T]\}^{-1} \tag{78}$$

where $\boldsymbol{P}_{\frac{1}{\hat{A}}} = \boldsymbol{I}_{MN} - \boldsymbol{A}(\boldsymbol{A}^H\boldsymbol{A})^{-1}\boldsymbol{A}^H$; $\boldsymbol{F} = [\boldsymbol{F}_1\boldsymbol{F}_1; \boldsymbol{F}_1\boldsymbol{F}_1]$, where $\boldsymbol{F}_1 = \boldsymbol{S}\boldsymbol{S}^H/J$; $\boldsymbol{W} = [\boldsymbol{W}_\theta, \boldsymbol{W}_r]$, where $\boldsymbol{W}_\theta$ and $\boldsymbol{W}_r$ are:

$$\boldsymbol{W}_\theta = [\frac{\partial \boldsymbol{a}_1}{\partial \theta_1}, \frac{\partial \boldsymbol{a}_2}{\partial \theta_2}, \cdots, \frac{\partial \boldsymbol{a}_K}{\partial \theta_K}] \tag{79}$$

$$\boldsymbol{W}_r = [\frac{\partial \boldsymbol{a}_1}{\partial r_1}, \frac{\boldsymbol{a}_2}{\partial r_2}, \cdots, \frac{\boldsymbol{a}_K}{\partial r_K}] \tag{80}$$

where $\boldsymbol{a}_k = \boldsymbol{a}_r(\theta_k) \otimes \boldsymbol{a}_t(\theta_k, r_k), k = 1, \cdots, K$.

4. Experimental Results, Performance and Complexity Analysis

4.1. Experimental Results and Performance Analysis

In this section, three incoherent targets are assumed to be in the far field of the monostatic FDA-MIMO radar systems. The numbers of elements of the transmitting array and receiving array are $M = 7$ and $N = 5$, respectively. The angle and range of the three targets are: $(\theta_1, r_1) = (-15°$,10 km), $(\theta_2, r_2) = (10°$,60 km) and $(r_2, \theta_2) = (35°$,80 km), respectively. The reflection coefficients are: $(\beta_1, \beta_2, \beta_3) = [1, 1, 1]$, and the Doppler frequencies are: $(f_1, f_2, f_3) =$ [100 Hz, 500 Hz, 2550 Hz]. The overall number of Monte Carlo trials in the simulation experiment is $L = 200$. The root mean square error

(RMSE) is employed to gauge the performance of the method. The RMSE of the range and angle estimated values are:

$$RMSE_r = \sqrt{\frac{1}{K}\frac{1}{L}\sum_{k=1}^{K}\sum_{l=1}^{l}(\hat{r}_{k,l} - r_k)^2} \tag{81}$$

$$RMSE_\theta = \sqrt{\frac{1}{K}\frac{1}{L}\sum_{k=1}^{K}\sum_{l=1}^{l}(\hat{\theta}_{k,l} - \theta_k)^2} \tag{82}$$

where $\hat{r}_{k,l}$ and $\hat{\theta}_{k,l}$ are the estimated values of the range and angle of k-th target for l-th Monte Carlo trial, respectively.

In the first experiment, we set the number of snapshots to $J = 100$ and the signal-to-noise ratio (SNR) to $SNR = 20$. The estimated values of angle and range are close to the set values, as shown in Figure 2. The stability and availability of the proposed method are reflected in this experiment.

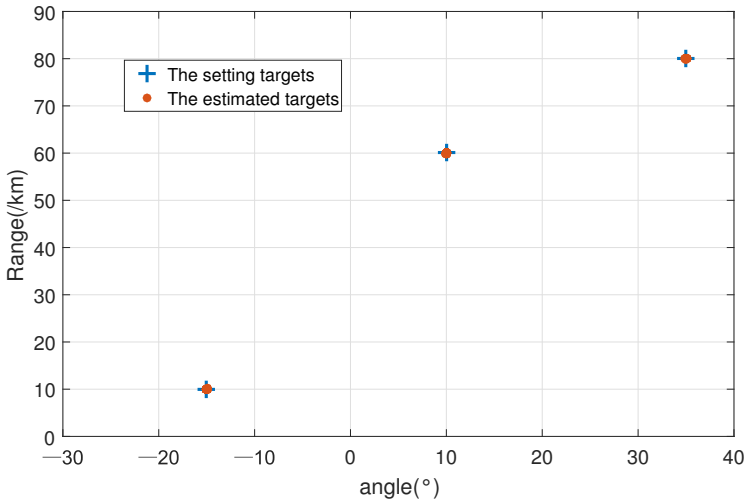


Figure 2. The calculated result of the method with $J = 100$, $SNR = 20$ dB.

In the second experiment, we investigate the range and angle parameter estimation performance of the proposed method under the different SNRs. The number of snapshots is set to $J = 100$. From Figures 3 and 4, it can be found that the proposed method outdoes the classic PARAFAC method [23], the ESPRIT method [15] and the unitary ESPRIT method [16], and the estimation performance becomes better as SNR increases. The reason for this is that the proposed method doubles the aperture of the array. Simultaneously, the proposed method performs similarly to the improved Gaussian random initialization method.

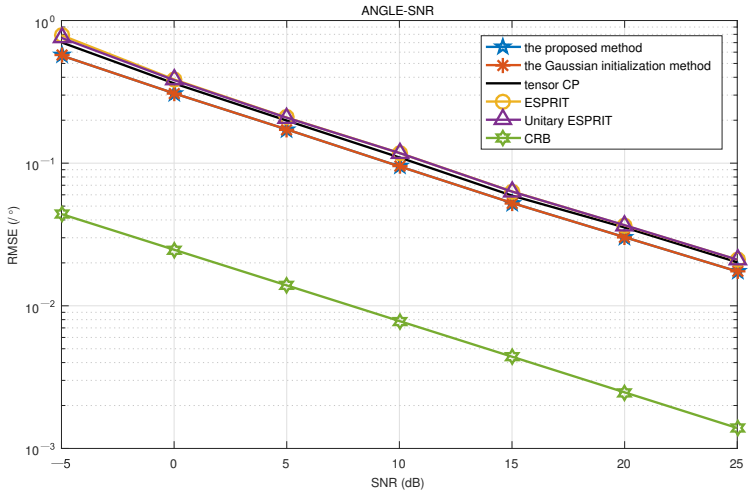


Figure 3. RMSE of angle estimation versus SNR.

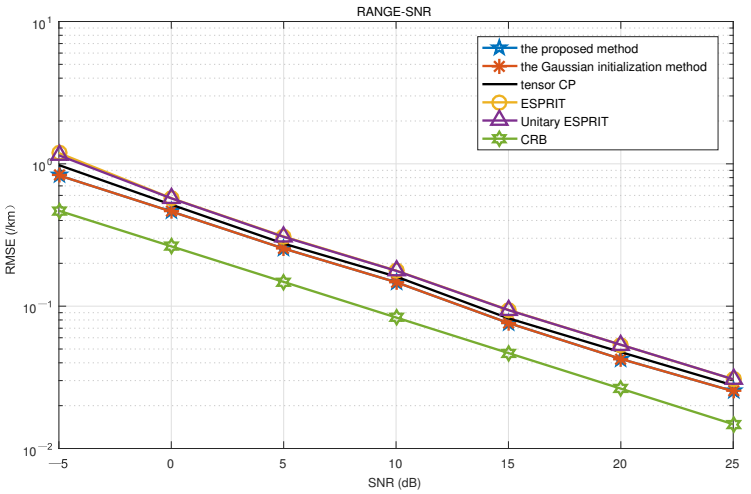


Figure 4. RMSE of range estimation versus SNR.

In the third experiment, we investigate the range and angle parameter estimation performance of the proposed method under the different numbers of snapshots. The SNR is set to 20. In Figures 5 and 6, it can be found that the estimated range and angle values of the proposed method are more accurate than those of the classic PARAFAC method [23], the ESPRIT method [15] and the unitary ESPRIT method [16], and the RMSE gradually lowers as the number of snapshots rises.

In the fourth experiment, we investigate the estimation performance of the proposed algorithm for the closed-target condition case. The three closed targets are $(\theta_1, r_1) = (30°, 60\text{ km})$, $(\theta_2, r_2) = (35°, 60\text{ km})$ and $(r_2, \theta_2) = (40°, 60\text{ km})$, and J is 100. In practice, if the targets are closed in space, the correlation between the column vectors of the orientation matrix becomes larger, which can make target separation difficult. In Figures 7 and 8, it can be observed that the proposed method has smaller RMSE values than the classic PARAFAC method [23], ESPRIT method [15] and unitary ESPRIT method [16] in the case of closed-target condition.

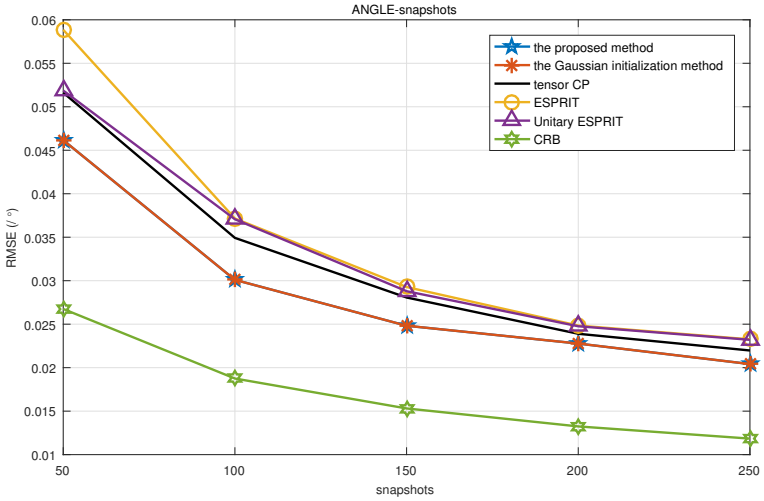


Figure 5. RMSE of angle estimation versus snapshots.

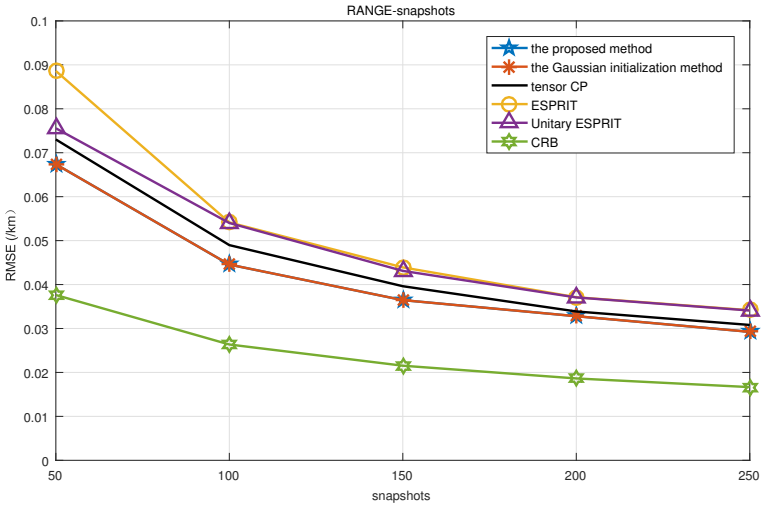


Figure 6. RMSE of range estimation versus snapshots.

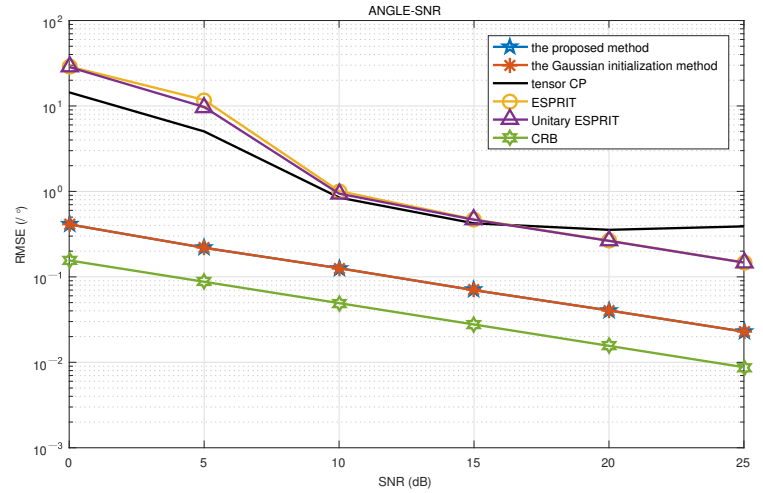


Figure 7. RMSE of angle estimation versus SNR with closed targets.

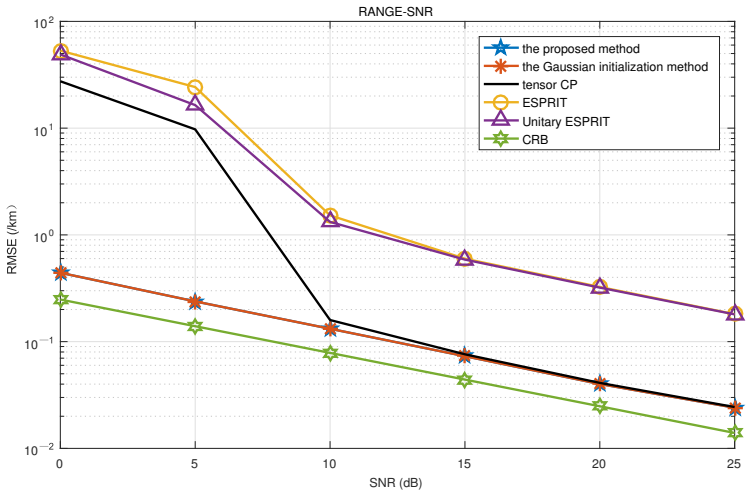


Figure 8. RMSE of range estimation versus SNR with closed targets.

4.2. Complexity Analysis

For the proposed method, the complexity of constructing the augmented output process is $O\{N^2M^2 + MNJ^2 + M^2N^2J\}$, the complexity of the initial estimation process of the factor matrix is $O\{8N^2M^2J + 4M^2N^2K + 6NK^2 + 2MK^3 + 8MNK^2 + 2NMKJ\}$, the computational complexity of each iteration process in the trilinear decomposition is $O\{3K^2 + 6KMNJ + 2K^2(2NJ + MJ + 2MN)\}$ and the number of iterations is n_1. The entire complexity of the proposed method is $O\{N^2M^2 + MNJ^2 + M^2N^2J + 8N^2M^2J + 4M^2N^2K + 6NK^2 + 2MK^3 + 8MNK^2 + 2NMKJ + n_1(6KMNJ + 3K^3 + 2K^2(2NJ + MJ + 2MN))\}$. The number of iterations in the proposed method is n_1. The overall complexity of the improved Gaussian random initialization algorithm is $O\{N^2M^2 + MNJ^2 + M^2N^2J + n_2(6KMNJ + 3K^3 + 2K^2(2NJ + MJ + 2MN))\}$. n_2 represents the number of iterations of the improved Gaussian random initialization algorithm. Usually, n_2 is larger than n_1, and often n_2 is much larger than n_1. Therefore, the overall complexity of the proposed method is less than that of the improved Gaussian random initialization method. Thus, as to verify the total complexity of the two algorithms, we performed 20,000 experiments and plotted the average time spent on each estimate by the two algorithms for these 20,000 experiments. In this experiment, the numbers of elements of the transmitter and receiver were $M = 7$ and $N = 5$, respectively. The SNR and the number of targets were 10 and 3, respectively. Figure 9 shows that the proposed method took less time than the improved Gaussian random initialization algorithm, and that the difference became more noticeable as the total number of snapshots rose. This proves that the method of estimating the factor matrix using the PM idea reduces the number of iterations of the trilinear decomposition process, thereby reducing the complexity of the algorithm.

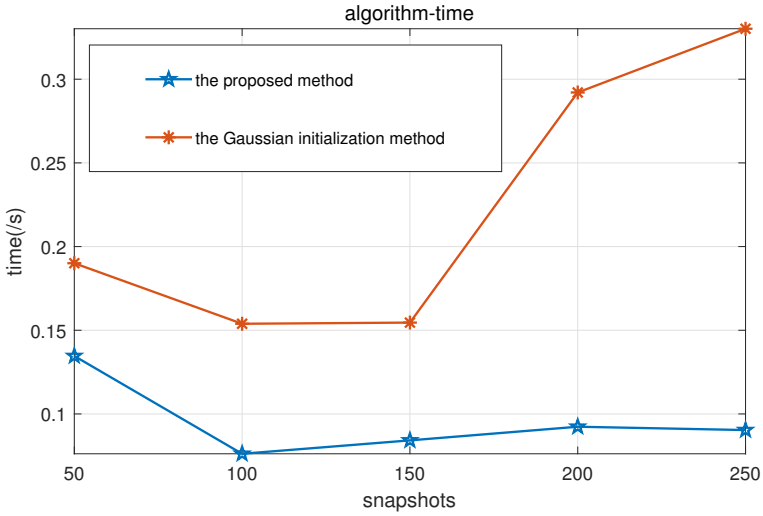


Figure 9. Average time required for each algorithm run.

5. Conclusions

In this paper, a joint range and angle estimation method based on fast improved PARAFAC decomposition for Monostatic FDA-MIMO radar was proposed. The proposed method constructs an augmented output with twice the aperture of the receive array via data expansion technique and unitary transformation. Then, the trilinear decomposition process is accelerated by factor matrix initialization and the direction matrix is obtained. Lastly, the range and angle estimated values are calculated by the LS fitting. In comparison with the classic PARARAC method, the proposed method can calculate more precise parameters and detect more targets. In addition, the proposed method uses the PM idea to calculate the factor matrix, avoiding the excessive number of iterations of the trilinear decomposition process.

Author Contributions: Conceptualization, W.W. and X.L.; methodology, W.W. and X.L.; writing—original draft preparation, W.W.; writing—review and editing, X.W. and X.L.; supervision, X.W.; funding acquisition, X.W. and J.S. All authors have read and agreed to the published version of the manuscript.

Funding: This work was supported by Natural Science Foundation of Hainan Province(number 621MS018), the National Natural Science Foundation of China Youth Science Fund Project (number 62101165), the National Natural Science Foundation of China (number 61861015 and 61961013), the Key Research and Development Program of Hainan Province (number ZDYF2019011), the National Key Research and Development Program of China (number 2019CXTD400), the Young Elite Scientists Sponsorship Program by CAST (number 2018QNRC001) and the Scientific Research Setup Fund of Hainan University (number KYQD(ZR) 1731).

Data Availability Statement: Not applicable.

Conflicts of Interest: The authors declare no conflict of interest.

References

1. Cong, J.; Wang, X.; Yan, C. CRB weighted source localization method based on deep neural networks in multi-UAV network. *IEEE Internet Things J.* 2022, *in press*.
2. Fishler, E.; Haimovich, A.; Blum, R. MIMO radar: An idea whose time has come. In Proceedings of the 2004 IEEE Radar Conference (IEEE Cat. No. 04CH37509), Philadelphia, PA, USA, 29 April 2004; pp. 71–78.
3. Li, J.; Stoica, P. *MIMO Radar Signal Processing*; Wiley-IEEE Press: New York, NY, USA, 2008.
4. Haimovich, A.M.; Blum, R.S.; Cimini, L.J. MIMO radar with widely separated antennas. *IEEE Signal Process. Mag.* **2008**, *25*, 116–129. [CrossRef]
5. Li, J.; Stoica, P. MIMO radar with colocated antennas. *IEEE Signal Process. Mag.* **2007**, *24*, 106–114. [CrossRef]
6. Zhou, S.; Liu, H.; Zhao, Y. Target spatial and frequency scattering diversity property for diversity MIMO radar. *Signal Process.* **2011**, *90*, 269–276. [CrossRef]

7. Mao, L.; Li, H.; Zhang, Q. Transmit subaperturing for MIMO radars with nested arrays. *Signal Process.* **2017**, *134*, 244–248. [CrossRef]
8. Wang, X.; Yang, L.T.; Meng, D. Multi-UAV cooperative localization for marine targets based on weighted subspace fitting in SAGIN environment. *IEEE Internet Things J.* **2021**, *9*, 5708–5718. [CrossRef]
9. Wang, H.; Xiao, P.; Li, X. Channel Parameter Estimation of mmWave MIMO System in Urban Traffic Scene: A Training Channel based Method. *IIEEE Trans. Intell. Transp. Syst.* **2022**, *4*, 1–9. [CrossRef]
10. Antonik, P.; Wicks, M.C.; Griffiths, H.D. Frequency diverse array radars. In Proceedings of the 2006 IEEE Conference on Radar, Verona, NY, USA, 24–27 April 2006; p. 3.
11. Wang, W.Q.; Thus, H.C. Transmit subaperturing for range and angle estimation in frequency diverse array radar. *IEEE Trans. Signal Process.* **2014**, *62*, 2000–2011. [CrossRef]
12. Huang, L.; Li, X.; Gong, P.C. Frequency diverse array radar for target range-angle estimation. *Int. J. Comput. Math. Electr. Electron. Eng.* **2016**, *35*, 1257–1270. [CrossRef]
13. Sammartino, P.F.; Baker, C.J.; Griffiths, H.D. Frequency diverse MIMO techniques for radar. *IEEE Trans. Aerosp. Electron. Syst.* **2013**, *49*, 201–222. [CrossRef]
14. Wang, W. Phased-MIMO Radar With Frequency Diversity for Range-Dependent Beamforming. *IEEE Sens. J.* **2013**, *13*, 1320–1328. [CrossRef]
15. Wen, F.; Shi, J.; Zhang, Z. Generalized spatial smoothing in bistatic EMVS-MIMO radar. *IEEE Access* **2022**, *193*, 108406. [CrossRef]
16. Liu, F.; Wang, X.; Huang, M. A novel unitary ESPRIT algorithm for monostatic FDA-MIMO radar. *Sensors* **2020**, *20*, 827. [CrossRef] [PubMed]
17. Xiong, J.; Wang, W.Q.; Gao, K. FDA-MIMO radar range–angle estimation: CRLB, MSE, and resolution analysis. *IEEE Trans. Aerosp. Electron. Syst.* **2017**, *54*, 284–294. [CrossRef]
18. Zhang, X.; Xu, Z.; Xu, L. Trilinear decomposition-based transmit angle and receive angle estimation for multiple-input multiple-output radar. *IET Radar Sonar Navig.* **2011**, *5*, 626–631. [CrossRef]
19. Zhang, X.; Li, J.; Chen, H. Trilinear decomposition-based two-dimensional DOA estimation algorithm for arbitrarily spaced acoustic vector-sensor array subjected to unknown locations. *Wirel. Pers. Commun.* **2012**, *67*, 859–877. [CrossRef]
20. Zhang, X.; Feng, G.; Yu, J. Angle–frequency estimation using trilinear decomposition of the oversampled output. *Wirel. Pers. Commun.* **2009**, *51*, 365–373.
21. Zhang, X.; Xu, D. Blind PARAFAC signal detection for polarization sensitive array. *EURASIP J. Adv. Signal Process.* **2007**, *2007*, 1–7. [CrossRef]
22. Shi, Y.; Zhang, X. Quadrilinear decomposition-based blind signal detection for polarization sensitive uniform square array. *Prog. Electromagn. Res.* **2008**, *87*, 263–278. [CrossRef]
23. Xu, T.; Yang, Y.; Huang, M. Tensor-based angle and range estimation method in monostatic FDA-MIMO radar. *Math. Probl. Eng.* **2020**, *2020*, 1–8. [CrossRef]
24. Cui, C.; Xu, J.; Gui, R. Search-free DOD, DOA and range estimation for bistatic FDA-MIMO radar. *IEEE Access* **2018**, *6*, 15431–15445. [CrossRef]
25. Guo, Y.; Wang, X.; Lan, X. Traffic Target Location Estimation Based on Tensor Decomposition in Intelligent Transportation System. *IEEE Trans. Intell. Transp. Syst.* 2022, *in press*.
26. Xu, L.; Wu, R.; Zhang, X. Joint two-dimensional DOA and frequency estimation for L-shaped array via compressed sensing PARAFAC method. *IEEE Access* **2018**, *6*, 37204–37213. [CrossRef]
27. Li, S.; Sun, Z.; Zhang, X. Joint DOA and frequency estimation for linear array with compressed sensing PARAFAC framework. *J. Circuits Syst. Comput.* **2017**, *26*, 1750136. [CrossRef]
28. Shi, J.; Yang, Z.; Liu, Y. On Parameter Identifiability of Diversity-Smoothing-Based MIMO Radar. *IEEE Trans. Aerosp. Electron. Syst.* **2021**, *58*, 1660–1675. [CrossRef]
29. Chen, W.; Xu, L.; Zhang, X. Two-dimensional DOA estimation of acoustic vector sensor array based on fast parallel factorization. *J. Nanjing Univ. Aeronaut. Astronaut.* **2021**, *53*, 130–135.
30. Wang, X.; Guo, Y.; Huang, M. Robust angle estimation method for non-circular targets in MIMO radar under mutual coupling conditions. *J. Commun.* **2019**, *40*, 144–150.
31. Zhang, X.; Cao, R.; Zhou, M. Noncircular-PARAFAC for 2D-DOA estimation of noncircular signals in arbitrarily spaced acoustic vector-sensor array subjected to unknown locations. *EURASIP J. Adv. Signal Process.* **2013**, *2013*, 1–10. [CrossRef]
32. Wang, X.; Wang, W.; Liu, J. Tensor-based real-valued subspace approach for angle estimation in bistatic MIMO radar with unknown mutual coupling. *Signal Process.* **2015**, *116*, 152–158. [CrossRef]
33. Xu, B.; Zhao, Y.; Cheng, Z. A novel unitary PARAFAC method for DOD and DOA estimation in bistatic MIMO radar. *Signal Process.* **2017**, *138*, 273–279. [CrossRef]
34. Li, J.; Zhou, M. Improved trilinear decomposition-based method for angle estimation in multiple-input multiple-output radar. *IET Radar Sonar Navig.* **2013**, *7*, 1019–1026. [CrossRef]
35. He, J.; Liu, Z. Two-dimensional direction finding of acoustic sources by a vector sensor array using the propagator method. *J. Nanjing Univ. Aeronaut. Astronaut.* **2008**, *88*, 2492–2499. [CrossRef]
36. Kolda, T.G.; Bader, B.W. Tensor decompositions and applications. *SIAM Rev.* **2009**, *51*, 455–500. [CrossRef]

37. Wang, X.; Wan, L.; Huang, M. Low-complexity channel estimation for circular and noncircular signals in virtual MIMO vehicle communication systems. *IEEE Trans. Veh. Technol.* **2020**, *69*, 3916–3928. [CrossRef]
38. Yao, A.M.; Rocca, P.; Wu, W. Synthesis of time-modulated frequency diverse arrays for short-range multi-focusing. *IEEE J. Sel. Top. Signal Process.* **2016**, *11*, 282–294. [CrossRef]
39. Shao, H.; Li, X.; Wang, W.Q. Time-invariant transmit beampattern synthesis via weight design for FDA radar. In Proceedings of the IEEE Radar Conference, Philadelphia, PA, USA, 2–6 May 2016; pp. 1–4.
40. Wang, Q.; Yu, D.; Zhu, Y. Angle-range estimation for bistatic FDA-MIMO radar viia tensor completion. *Telecommun. Radio Eng.* **2020**, *79*, 753–768. [CrossRef]
41. Xu, J.; Liao, G.; Zhu, S. Joint range and angle estimation using MIMO radar with frequency diverse array. *IEEE Trans. Signal Process.* **2015**, *63*, 3396–3410. [CrossRef]
42. Zoltowski, M.D.; Haardt, M.; Mathews, C.P. Closed-form 2-D angle estimation with rectangular arrays in element space or beamspace via unitary ESPRIT. *IEEE Trans. Signal Process.* **1996**, *44*, 316–328. [CrossRef]
43. Sidiropoulos, N.D.; Bro, R.; Giannakis, G.B. Parallel factor analysis in sensor array processing. *IEEE Trans. Signal Process.* **2000**, *48*, 2377–2388. [CrossRef]